

Extraction of α_s from deep inelastic scattering at large x

A. Courtoy*

*IFPA, AGO Department, Université de Liège,
Bât. B5, Sart Tilman B-4000 Liège, Belgium*

S. Liuti†

*Department of Physics,
University of Virginia,
382 McCormick Rd.,
Charlottesville, VA 22904, USA*

(Dated: May 18, 2021)

Abstract

We present an analysis of the role of the running coupling constant at the intersection of perturbative and nonperturbative QCD. Although the approaches that have been considered so far in these two regimes appear to be complementary to each other, a unified description might derive through the definition of the effective coupling, as they both provide ways of analyzing its freezing at low values of the scale. We extract the effective coupling from all available experimental data on the unpolarized structure function of the proton, F_2^p , at large values of Bjorken x , including the resonance region. We suggest that parton-hadron duality observed in this region can be explained if nonperturbative effects are included in the coupling constant. The outcome of our analysis is a smooth transition from perturbative to nonperturbative QCD physics, embodied in the running of the coupling constant at intermediate scales.

PACS numbers:

*Electronic address: Aurore.Courtoy@ulg.ac.be

†Electronic address: sl4y@virginia.edu

1. Hard processes are described in QCD by envisaging a perturbative stage (PQCD) where a hard collision involving quark and gluons occurs, followed by a nonperturbative stage characterizing hadron structure. For example, in Deep Inelastic Scattering (DIS) the hard scattering part of the process, $\gamma^* q \rightarrow X$, can be presently described using splitting functions up to next-to-next-to-leading order (NNLO) [1, 2], and Wilson coefficients functions up to N³LO [3]. The large distance part is described by the Parton Distribution Functions (PDFs), which have to be extracted from fits of high energy experimental data. PDF parametrizations along with their uncertainties have been obtained applying this framework up to NNLO, by a number of collaborations (see review in [4]). NLO PDFs are also important for the comparison with data from, *e.g.*, collider processes which are only known up to NLO, and when using Monte Carlo event generators.

Although DIS stands out as the most accurately described process in a QCD factorized scenario, at large Bjorken x large logarithms appear in the PQCD description that need to be resummed in order to ensure that the perturbative approach can be consistently extended. In this region power corrections of both kinematical (Target Mass Corrections, TMCs) and dynamical (Higher Twists, HT) origin also affect the extraction of PDFs. They are intertwined with Large x Resummation (LxR), and the factorization framework is no longer expected to apply straightforwardly [5].

Early experimental observations indeed suggested that in specific kinematical regimes both the perturbative and nonperturbative stages arise almost ubiquitously, in the sense that the nonperturbative description tracks, in average, the behavior of the perturbative one. In inclusive eP scattering at large x , a duality between the low-energy and high-energy behaviors of a same observable, *i.e.*, the unpolarized structure function, F_2^p was observed by Bloom and Gilman who established a connection between the structure function in the nucleon resonance region and that in the deep inelastic continuum [6, 7]. F_2^p , when averaged over the resonance region, was found to be equivalent to the continuation of the deep inelastic curve in this region. This concept is known as *parton-hadron duality*: the resonances are not a separate entity but they are an intrinsic part of the scaling behavior of the structure function. Note that here duality implies an equality in average between resonances and scaling curve, the average being taken at fixed four-momentum transfer, $Q^2 \geq 1 \text{ GeV}^2$, over the same range in the scaling variable, x . This behavior can be taken as signaling a natural continuation of the perturbative to the nonperturbative representation.

Although Bloom–Gilman duality was observed at the inception of QCD, quantitative analyses could be attempted only more recently, having at disposal the extensive, high precision data from Jefferson Lab [8].

In this paper, to evaluate the impact of LxR, we perform an analysis of inclusive eP scattering data at large x , including resonance data. To handle the latter, we follow closely the analysis of Ref. [9], where the implications of parton-hadron duality were explored in the context of a systematic PQCD based analysis including besides LxR, TMCs and HT contributions or, more generally, the evidence for nonperturbative inserts, which are required to achieve a fully quantitative fit. Here the relevant kinematical variables are: $x = Q^2/2M\nu$ (M being the proton mass and ν the energy transfer in the lab system), the four-momentum transfer, Q^2 , and the invariant mass for the proton, P , and virtual photon, q , system, $W^2 = (P + q)^2$ ($W^2 = Q^2(1/x - 1) + M^2$). For large values of Bjorken $x \geq 0.5$, and Q^2 in the multi-GeV² region, one has $W^2 \leq 5 \text{ GeV}^2$, *i.e.*, the cross section is dominated by resonance formation.

As first pointed out in Refs. [9, 10], the extension of PQCD evolution to large x must also

include LxR effects. A consequence of LxR is that as x increases there is a shift to lower values of the scale at which α_s is calculated (see for instance Ref. [11] or the classical review in Ref.[12]). At large x and low W^2 , this shift requires a freezing of the coupling constant in the infrared region.

The key result in the present work is that, by turning this argument around, or by using the fact that our analysis, through LxR, is regulated by the value of the QCD coupling in the infrared region, we can extract such coupling from experimental data. In our analysis canonical higher-twist terms are suppressed in that their separate contributions to the perturbative curve to be compared to the large x data is negligible. However, nonperturbative effects are present as they become absorbed in the coupling's infrared behavior.

The extracted coupling we obtain is consistent with schemes of scale fixing in which α_s can be extended to the entire Q^2 domain. Various frameworks have been proposed where the effective coupling is free of the Landau pole, *e.g.*, the BLM scheme [13] and its recent extension using the Principle of Maximum Conformality [14], methods based on the analyticity properties of α_s [15, 16], and finally, including nonperturbative effects [17–20] (see also Refs. [21, 22] where α_s was defined introducing nonperturbative effects fixed by a physical set of parameters). While the focus of the present manuscript is on suggesting a way of extracting the running coupling from data, more detailed future studies will be dedicated to connecting our approach to the mentioned schemes.

2. In order to evaluate the effect of LxR we perform a fit of all available large x , eP inclusive scattering data. We start from standard parametrizations of the PDFs, and we consider systematically the effects of TMCs, and perturbative evolution using either NLO or next-to-leading log (NLL) resummed coefficient functions, *i.e.*, with and without LxR. Note that the scope of the present fit is not towards a global analysis, but to assess the possible interplay among the different components that impact Q^2 evolution at large x , including LxR, TMCs, and HTs. In the resonance region, $W^2 \leq 4 \text{ GeV}^2$, we consider averages of both data and theoretical evaluations by comparing limited intervals defined as,

$$R^{\text{exp/th}}(Q^2) = \frac{\int_{x_{\min}(W^2=4\text{GeV}^2)}^{x_{\max}(W^2=1.2\text{GeV}^2)} dx F_2^{\text{exp}}(x, Q^2)}{\int_{x_{\min}(W^2=4\text{GeV}^2)}^{x_{\max}(W^2=1.2\text{GeV}^2)} dx F_2^{\text{th}}(x, Q^2)} . \quad (1)$$

In the present analysis, we use, for F_2^{exp} , the data from JLab (Hall C, E94110) [23] reanalyzed (binning in Q^2 and x) as explained in [24] as well as the SLAC data [25]. The values of Q^2 and the average values of x for each interval are given in Table I. The function F_2^{th} is the theoretical evaluation which is the same in both the DIS and resonance, Eq. (1), regions. Notice that if Eq. (1) is equal to 1, duality is fulfilled. Since x is integrated over the entire resonance region, we are considering *global duality*.

The OPE formulation of quark-hadron duality [26] suggests that the higher-twist contributions to the scaling structure function would either be small or cancel otherwise duality would be strongly violated. However, the role of the higher-twist terms is still unclear since they would otherwise be expected to dominate the cross section at $x \rightarrow 1$. To answer the question of the nature of a dual description, two complementary approaches have been adopted. The first is the nonperturbative model's view on the scaling of the structure functions at low-energies [27–29]; the second approach consists in a perturbative analysis [9, 10, 30], that through LxR provides a scenario by which the effect of HTs can be suppressed in a fully quantitative fit at large x . It is this second approach that we will follow in this paper.

We evaluate F_2^{th} taking into account perturbative evolution at NLO, and introduce subsequently the effects of TMCs, and LxR. Since only valence quarks distributions are relevant in our kinematics, we consider only the Non Singlet (NS) sector,

$$F_2^{NS}(x, Q^2) = xq(x, Q^2) + \frac{\alpha_s}{4\pi} \sum_q \int_x^1 dz B_{\text{NS}}^q(z) \frac{x}{z} q\left(\frac{x}{z}, Q^2\right) \quad , \quad (2)$$

The PDFs, $q(x, Q^2)$, are taken from current parametrizations. We have chosen to present results using the MSTW08 set at NLO as initial parametrization [31]. We have checked that there were no significant discrepancies when using other sets, *i.e.*, CTEQ6 [32] and the dynamical GJRfVNS [33]. The function B_{NS}^q is the Wilson coefficient function for quark-quark.

By evaluating the ratios $R_{\text{exp/th}}$, using current parametrizations, one finds a sensible deviation from the data, even when the theoretical uncertainty from the parametrizations is included (Figure 1). One possible explanation is in the lack of accuracy in the PDF parametrizations in the large x , low W^2 domain, since most groups implement much larger thresholds for W^2 . The way to a fully quantitative fit would then start from re-fitting the large x data with new appropriate sets of PDFs, and simultaneously accounting for both TMCs, and LxR. The number of parameters, and the uncertainty associated with this procedure would however be dauntingly increasing. For this reason, it is therefore necessary to take the preparatory step, conducted with the present analysis, of assessing the relative weight of the different contributions.

The additional corrections due to the finite mass of the initial nucleon, or the TMCs, are included directly in $F_2^{NS, \text{th}}$ as [34] (see also review in [35]),

$$F_2^{NS(TMC)}(x, Q^2) = \frac{x^2}{\xi^2 \gamma^3} F_2^\infty(\xi, Q^2) + 6 \frac{x^3 M^2}{Q^2 \gamma^4} \int_\xi^1 \frac{d\xi'}{\xi'^2} F_2^\infty(\xi', Q^2), \quad (3)$$

where $F_2^\infty \equiv F_2^{NS}$ is the structure function in the absence of TMC. Since TMC should in principle be applied also to the HT, we disregard terms of $\mathcal{O}(1/Q^4)$ [36]. Note that the expansion in Eq. (3) is valid for Q^2 larger than $\approx 1 \text{ GeV}^2$. TMCs move the ratio closer to unity, as represented by the open green diamonds in Fig. 1. Uncertainties on TMCs are very small [36]. However a larger error might arise from the procedure used to account for TMCs [37]. Studies of the sensitivity to this procedure are on their way and will be published elsewhere. At this stage, by including only TMCs and standard PDF parametrizations, we still observe a large discrepancy with the data.

Next, we consider LxR effects. A major consequence of LxR is a shift of the scale at which α_s is calculated to lower values, with increasing z (see for instance Refs. [11, 12, 38]). This introduces a model dependence within the PQCD approach in that the value of the QCD running coupling in the infrared region is regulated by LxR so as to satisfy duality. In other words, LxR contains an additional degree of freedom, gathered in the definition of the coupling constant, to tune the scaling structure functions.

LxR arises formally from terms containing powers of $\ln(1-z)$, z being the longitudinal variable in the evolution equations, that are present in the Wilson coefficient functions $B_{\text{NS}}^q(z)$, in Eq. (2). To NLO and in the $\overline{\text{MS}}$ scheme, the Wilson coefficient function for quarks reads,

$$B_{\text{NS}}^q(z) = \left[\hat{P}_{qq}^{(0)}(z) \left\{ \ln\left(\frac{1-z}{z}\right) - \frac{3}{2} \right\} + \text{E.P.} \right]_+ \quad , \quad (4)$$

Q^2 [GeV ²]	x_{ave}	$I^{\text{exp}}(Q^2)$
1.75	0.516	6.994×10^{-2}
2.5	0.603	4.881×10^{-2}
3.75	0.702	2.356×10^{-2}
5.	0.753	1.267×10^{-2}
6.5	0.800	0.685×10^{-2}
4.	0.712	2.045×10^{-2}
5.	0.755	1.255×10^{-2}
6.	0.787	0.802×10^{-2}
7.	0.812	0.531×10^{-2}
8.	0.832	0.363×10^{-2}

TABLE I: Upper block: Integrals of JLab data from Refs. [23, 24], appearing in the numerator of Eq. (1). The first column shows the average values of x for each bin. Lower block: SLAC data [25].

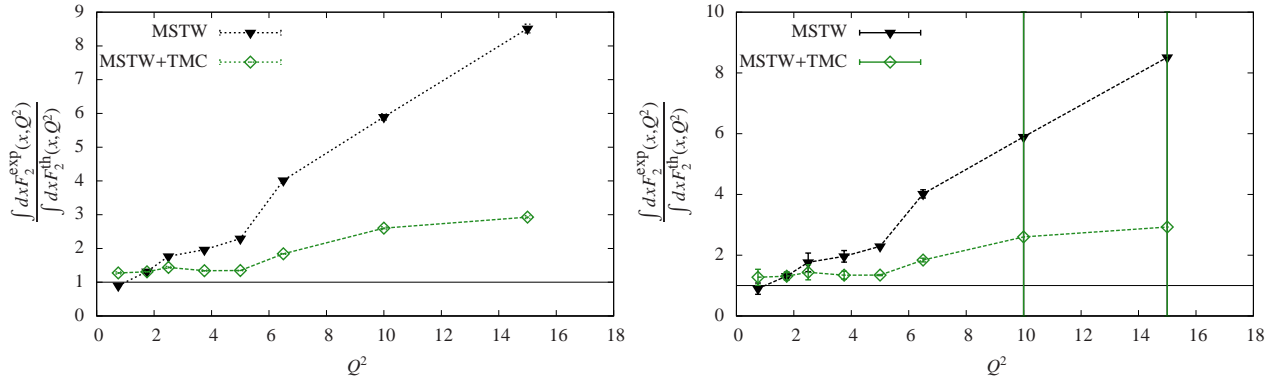


FIG. 1: Ratio $R^{\text{exp/th}}(Q^2)$ of Eq. (1) where the theoretical analysis includes PQCD evolution using the MSTW08 PDF set (black triangle), and MSTW08 PDF set plus TMCs (open green diamonds). Ratios with error bars on data integrated in quadrature ; right panel: ratios with weighted error bars on data integrated in quadrature.

where E.P. means end points and $[\dots]_+$ denotes the standard plus-prescription. The function $\hat{P}_{qq}^{(0)}(z)$ is the LO splitting function for quark-quark. The logarithmic terms, *i.e.*, $\ln(1-z)$, in $B_{\text{NS}}^q(z)$ become very large at large x values. They need to be resummed to all orders in α_s . Resummation was first introduced by linking this issue to the definition of the correct kinematical variable that determines the phase space for the radiation of gluons at large x . This was found to be $\widetilde{W}^2 = Q^2(1-z)/z$, instead of Q^2 [11, 39]. As a result, the argument of the strong coupling constant becomes z -dependent [40],

$$\alpha_s(Q^2) \rightarrow \alpha_s\left(Q^2 \frac{(1-z)}{z}\right) . \quad (5)$$

In this procedure, however, an ambiguity is introduced, related to the need of continuing the value of α_s for low values of its argument, *i.e.*, for $z \rightarrow 1$ [41]. Since the size of this ambiguity is of the same order as the higher-twist corrections, it has been considered, in a previous work [42], as a source of theoretical error or higher order effects. We investigate

the effect induced by changing the argument of α_s on the behavior of the $\ln(1-z)$ -terms in the convolution Eq. (2), and resum those terms as

$$\ln(1-z) = \frac{1}{\alpha_{s,\text{LO}}(Q^2)} \int^{Q^2} d\ln Q^2 [\alpha_{s,\text{LO}}(Q^2(1-z)) - \alpha_{s,\text{LO}}(Q^2)] \equiv \ln_{\text{LxR}} \quad , \quad (6)$$

including the complete z dependence of $\alpha_{s,\text{LO}}(\tilde{W}^2)$ to all logarithms.¹ Note that we are using three different concepts of order expansions. The present analysis is conducted to *next-to-leading order* (we evolve the PDF sets to NLO), to *leading-twist* (we consider the LT PDFs only) and to *all logarithms* (we include $\alpha_{s,\text{LO}}(\text{scale})$ to all logarithms). This resummation is easily understood when considering the first term of the expansion of $\alpha_s(\tilde{W}^2)$ in $\ln((1-z)/z)$,

$$\alpha_s(\tilde{W}^2) = \alpha_s(Q^2) - \frac{\beta_0}{4\pi} \ln\left(\frac{1-z}{z}\right) \alpha_s^2(Q^2), \quad (7)$$

as proposed in Ref. [40]. To all logarithms, the convolution becomes

$$F_2^{NS,\text{Resum}}(x, Q^2) = xq(x, Q^2) + \frac{\alpha_s}{4\pi} \sum_q \int_x^1 dz B_{\text{NS}}^{\text{Resum}}(z) \frac{x}{z} q\left(\frac{x}{z}, Q^2\right), \quad (8)$$

where,

$$B_{\text{NS}}^{\text{Resum}} = B_{\text{NS}}^q(z) - \hat{P}_{qq}^{(0)}(z) \ln(1-z) + \hat{P}_{qq}^{(0)}(z) \ln_{\text{LxR}}. \quad (9)$$

Using $F_2^{NS,\text{Resum}}$ plus TMCs, in Eq. (1), will make the ratio R decreases substantially, essentially leaving no space for HT terms. This is due in our approach mostly to the change of the argument of the running coupling constant. At fixed Q^2 , in the integration over $x < z < 1$, the scale $\tilde{W}^2 = Q^2(1-z)/z$ is shifted and can reach low values, where the running of the coupling constant starts blowing up. At this stage, our analysis requires nonperturbative information. A way to address this issue is to set a maximum value for the longitudinal momentum fraction, z_{max} , which defines a limit from which nonperturbative effects have to be accounted for, and to cut α_s at the corresponding scale, $\tilde{W}^2(z_{\text{max}}) = Q^2(1-z_{\text{max}})/z_{\text{max}}$. Larger values of z_{max} correspond to lower values at which the scale should be cut in the analysis, meaning that the perturbative value can be used. As we show later, large z_{max} occurs in the data at large Q^2 , therefore the effect of the shift in scale gets smaller.

The functional form \ln_{LxR} is therefore slightly changed. Two distinct regions can be studied: the “running” behavior in $x < z < z_{\text{max}}$ and the “steady” behavior $z_{\text{max}} < z < 1$,

$$\begin{aligned} F_2^{NS,\text{Resum}}(x, z_{\text{max}}, Q^2) = & xq(x, Q^2) + \frac{\alpha_s}{4\pi} \sum_q \left\{ \int_x^1 dz \left[B_{\text{NS}}^q(z) - \hat{P}_{qq}^{(0)}(z) \ln(1-z) \right] \right. \\ & \left. + \int_x^{z_{\text{max}}} dz \hat{P}_{qq}^{(0)}(z) \ln_{\text{LxR}} + \ln_{\text{LxR}, \text{max}} \int_{z_{\text{max}}}^1 dz \hat{P}_{qq}^{(0)}(z) \right\} \frac{x}{z} q\left(\frac{x}{z}, Q^2\right). \end{aligned} \quad (10)$$

¹ The terms proportional to $\ln z$ are not divergent at $z \rightarrow 1$.

z_{\max} appears therefore as a free parameter in our analysis. A possible criterion to constrain it is to fit the large x data assuming a null direct contribution to the structure function from the dynamical HTs namely, for each Q^2 bin we define z_{\max} by varying $R^{\text{exp/th}}$ as a function of z_{\max} , so that

$$R^{\text{exp/th}}(z_{\max}, Q^2) = \frac{\int_{x_{\min}}^{x_{\max}} dx F_2^{\text{exp}}(x, Q^2)}{\int_{x_{\min}}^{x_{\max}} dx F_2^{NS, \text{Resum}}(x, z_{\max}, Q^2)} = \frac{I^{\text{exp}}}{I^{\text{Resum}}} = 1 \quad . \quad (11)$$

In Eq. (11), $F_2^{NS, \text{Resum}}(x, z_{\max}, Q^2)$ was evaluated including TMCs, resummation to all log, and setting possible dynamical HT contributions to zero. The latter get, however, absorbed in the coupling's infrared behavior. More precisely, the suppression of HTs in the structure function is compensated by the behavior of α_s in the infrared region. As a result, contrarily to what originally deduced in, *e.g.*, Ref. [43], a definite role of nonperturbative corrections is obtained, pointing at the fact that duality, defined on the basis of a dominance of single parton scattering, *i.e.*, suppression of final state interactions, might indeed be broken.

Results are represented by the red hexagons in Fig. 2. The integrals values are given in Tab. II together with the corresponding values for z_{\max} . Since, for the largest values of Q^2 , $Q^2 = 10, 15 \text{ GeV}^2$, outside the resonance region, on Fig. 1, z_{\max} becomes closer to 1, we do not consider those data points in what follows.

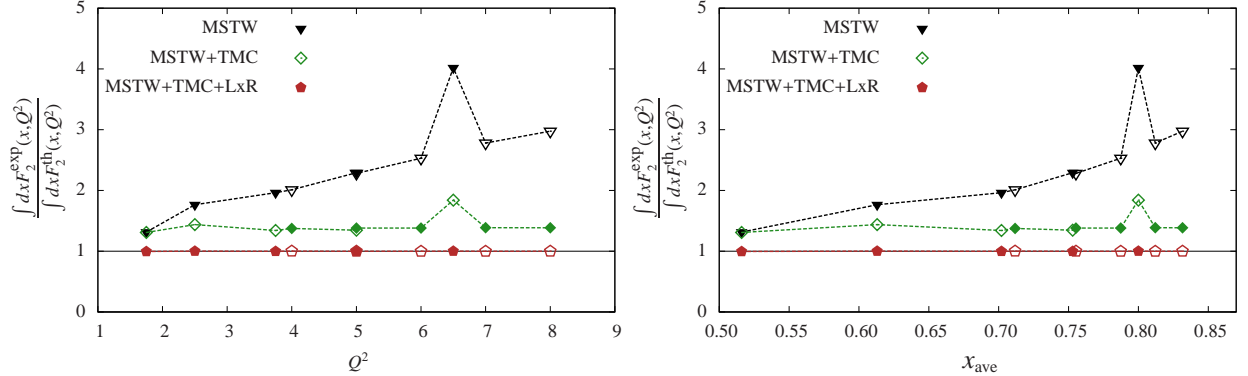


FIG. 2: The ratio $R^{\text{exp/th}}(x_{\text{ave}}, Q^2)$ as a function of Q^2 , on the left pannel, and as a function of x_{ave} on the right. Same as Fig. 1 but with the red hexagon representing the LxR results of Tab. II. The key shows the results corresponding to JLab data. The open triangle, full diamonds and open hexagons corresponds to SLAC data.

3. Based on the results of our analysis of large x data including TMCs and LxR, we now extract α_s by assuming that it runs from the onset of a minimal scale which is determined from the comparison with data, and it is frozen from that minimal scale downward to the real photon limit (scale=0 GeV^2). As one can see from Table II, data in the resonance region are crucial for this determination.

In Fig. 3 we show our extracted value $\alpha_{s, \text{NLO}}(\text{scale})$ where we used the $\overline{\text{MS}}$ scheme outside the IR region, for the same value of Λ throughout this paper. α_s was obtained as an exact solution to NLO [21]. Our theoretical error band is defined by the shift in z_{\max} from the

Q^2 [GeV ²]	$I^{\text{exp}}(Q^2)$	$I^{(0),\text{DIS}}(Q^2)$	$I^{(0),\text{DIS+TMC}}(Q^2)$	$I^{\text{Resum}}(z_{\text{max}}, Q^2)$	z_{max}
1.75	6.994×10^{-2}	5.316×10^{-2}	5.345×10^{-2}	7.025×10^{-2}	0.63
2.5	4.881×10^{-2}	2.765×10^{-2}	3.393×10^{-2}	4.872×10^{-2}	0.745
3.75	2.356×10^{-2}	1.201×10^{-2}	1.756×10^{-2}	2.359×10^{-2}	0.76
5.	1.267×10^{-2}	0.553×10^{-2}	0.942×10^{-2}	1.270×10^{-2}	0.79
6.5	0.685×10^{-2}	0.170×10^{-2}	0.372×10^{-2}	0.683×10^{-2}	0.9
4.	2.045×10^{-2}	1.017×10^{-2}	1.487×10^{-2}	2.041×10^{-2}	0.79
5.	1.255×10^{-2}	0.550×10^{-2}	0.909×10^{-2}	1.255×10^{-2}	0.811
6.	0.802×10^{-2}	0.317×10^{-2}	0.581×10^{-2}	0.803×10^{-2}	0.825
7.	0.531×10^{-2}	0.191×10^{-2}	0.383×10^{-2}	0.532×10^{-2}	0.837
8.	0.363×10^{-2}	0.122×10^{-2}	0.262×10^{-2}	0.363×10^{-2}	0.845

TABLE II: Integrals at each stage. In the last columns: the value z_{max} associated with $I^{\text{Resum}}(z_{\text{max}}, Q^2)$.

different bins displayed in Table II namely,

$$\alpha_{s,\text{NLO}} \left(Q_i^2 \frac{(1 - z_{\text{max},i})}{z_{\text{max},i}} \right) \quad \text{for} \quad i = 1, \dots, 10 \quad , \quad (12)$$

i corresponds to the data points. Including this error band, our extracted frozen value of the coupling constant is, using the MSTW08 PDF set for the analysis,

$$0.1337 \leq \frac{\alpha_{s,\text{NLO}}(\text{scale} \rightarrow 0\text{GeV}^2)}{\pi} \leq 0.1839 \quad . \quad (13)$$

In the figure we also report values from the extraction using polarized eP scattering data in Ref. [44–47]. These values represent the first extraction of an effective coupling in the IR region that was obtained by analyzing the data relevant for the study of the GDH sum rule. To extract the coupling constant, the $\overline{\text{MS}}$ expression of the Bjorken sum rule up to the 5th order in alpha (calculated in the $\overline{\text{MS}}$ scheme) was used. In order to compare with our extraction using the F_2^p observable, the finite value for $\alpha_s(0)$ found in [45–47] was rescaled in [44] assuming the validity of the commensurate scale relations [47] in the entire range of the scale entering the analysis. The agreement with our analysis which is totally independent, is impressive.

4. In conclusion, we presented an extraction of α_s using eP scattering data at large x . A careful analysis of all the contributions appearing at large x including TMCs and LxR, was performed. The central value for $\alpha_s(Q^2 < 1\text{GeV}^2)/\pi$ was found to be 0.1588. This value is in agreement with the extraction from the GDH sum rule analysis [44–46].

When considering PQCD observables at low scales, we implicitly face an interpretation problem. In the multi-GeV² region and at large- x , where the resonances lie, perturbative QCD is pushed to its limits. Both higher terms in the perturbative expansion of that observable, and power corrections need be taken into account. In the present approach, this transition is taken into account by re-interpreting the running coupling constant, at the scale of transition instead. By tuning the scaling structure functions to the averaged data in the resonance region, we parametrize the realization of duality through an infrared fixed-point

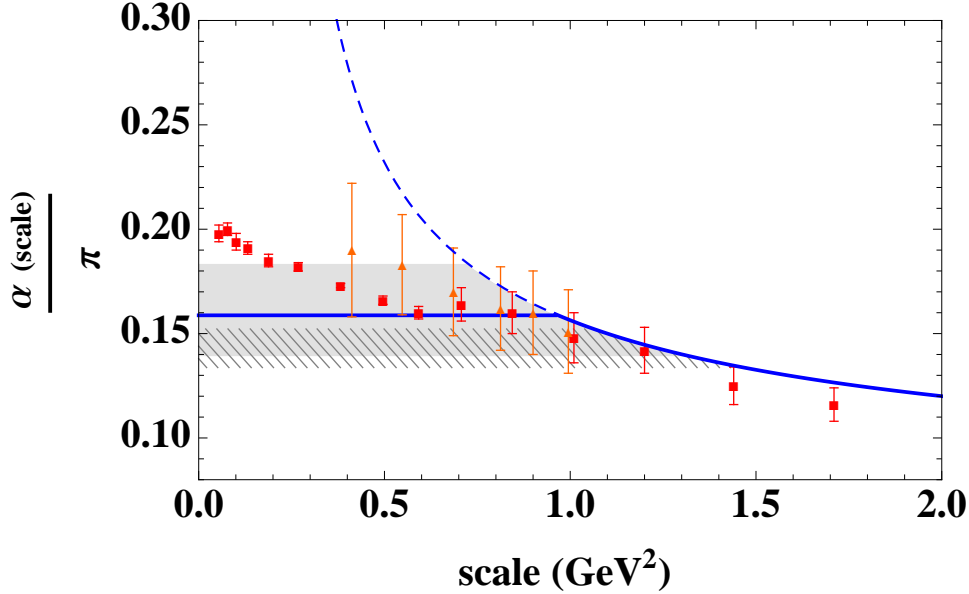


FIG. 3: (color online) Extraction of α_s . The blue dashed curve represents the exact NLO solution for the running coupling constant in $\overline{\text{MS}}$ scheme. The solid blue curve represents the coupling constant obtained from our analysis using inclusive electron scattering data at large x . Owing to large x resummation, at lower values of the scale, $\alpha_s = \alpha_{s,\text{NLO}}(\text{min})$ is frozen as explained in the text. The grey area represents the region where the freezing occurs for JLab data, while the hatched area corresponds the freezing region determined from SLAC data. This error band represents the theoretical uncertainty in our analysis. We also plot results extrapolated [44] from the recent analysis in Refs. [45, 46]: the red squares correspond to α_s extracted from Hall B CLAS EG1b, with statistical uncertainties; the orange triangles corresponds to Hall A E94010 / CLAS EG1a data, the uncertainty here contains both statistics and systematics.

below which the strong coupling constant stops running. The value we have found for the transition scale is situated around 1 GeV^2 . The uncertainties on that value are, however, still important.

We report an interesting observation that by connecting the values of the coupling using two different observables and schemes, namely the g_1 scheme from the GDH sum rule extraction, and our $\overline{\text{MS}}$ based extraction, we obtain an excellent agreement by simply extending the commensurate scale relations to the IR region (see also [48, 49]). While our conclusion ensues from a perturbative analysis, in the near future, we will explore the role of nonperturbative effective couplings as well. An interesting avenue is provided in this direction by the evaluation of the strong coupling constant in the infrared region using the AdS/CFT conjecture that was recently performed in Ref. [47].

The importance of finite couplings has been highlighted many times in the Literature, see, *e.g.*, [14] and references therein. Our analysis, would allow in principle, to extract from a fit the nonperturbative parameters often present in the proposed functional forms for the running of α_s , *e.g.*, in Refs. [15, 17, 18].

We are grateful to Vicente Vento and Stan Brodsky for many discussions and invaluable

advice. We also thank Alexandre Deur and Jian Ping Chen for useful discussions and for sending us their extracted values of the coupling constant, Peter Monaghan and Donal Day for directing us to the large x database. The support of Gruppo III of INFN, Laboratori Nazionali di Frascati, where part of the manuscript was completed is also wholeheartedly acknowledged. This work was funded by the Belgian Fund F.R.S.-FNRS via the contract of Charge de recherches (A.C.), and by U.S. D.O.E. grant DE-FG02-01ER4120 (S.L.).

-
- [1] S. Moch, J. Vermaseren, and A. Vogt, Nucl.Phys. **B688**, 101 (2004), hep-ph/0403192.
 - [2] A. Vogt, S. Moch, and J. Vermaseren, Nucl.Phys. **B691**, 129 (2004), hep-ph/0404111.
 - [3] J. Vermaseren, A. Vogt, and S. Moch, Nucl.Phys. **B724**, 3 (2005), hep-ph/0504242.
 - [4] S. Forte and G. Watt (2013), 1301.6754.
 - [5] G. Corcella and L. Magnea, Phys.Rev. **D72**, 074017 (2005), hep-ph/0506278.
 - [6] E. D. Bloom and F. J. Gilman, Phys.Rev.Lett. **25**, 1140 (1970).
 - [7] E. D. Bloom and F. J. Gilman, Phys.Rev. **D4**, 2901 (1971).
 - [8] W. Melnitchouk, R. Ent, and C. Keppel, Phys.Rept. **406**, 127 (2005), hep-ph/0501217.
 - [9] S. Liuti, Int.J.Mod.Phys.Conf.Ser. **04**, 190 (2011), 1108.3266.
 - [10] N. Bianchi, A. Fantoni, and S. Liuti, Phys.Rev. **D69**, 014505 (2004), hep-ph/0308057.
 - [11] S. J. Brodsky and G. P. Lepage, SLAC-PUB-2447 (1979).
 - [12] M. Pennington, Rept.Prog.Phys. **46**, 393 (1983).
 - [13] S. J. Brodsky, G. P. Lepage, and P. B. Mackenzie, Phys.Rev. **D28**, 228 (1983).
 - [14] X.-G. Wu, S. J. Brodsky, and M. Mojaza (2013), 1302.0599.
 - [15] D. Shirkov and I. Solovtsov, Phys.Rev.Lett. **79**, 1209 (1997), hep-ph/9704333.
 - [16] K. Milton, I. Solovtsov, and O. Solovtsova, Phys.Lett. **B415**, 104 (1997), hep-ph/9706409.
 - [17] J. M. Cornwall, Phys.Rev. **D26**, 1453 (1982).
 - [18] C. S. Fischer and R. Alkofer, Phys.Rev. **D67**, 094020 (2003), hep-ph/0301094.
 - [19] G. Prosperi, M. Raciti, and C. Simolo, Prog.Part.Nucl.Phys. **58**, 387 (2007), hep-ph/0607209.
 - [20] A. Aguilar, D. Binosi, J. Papavassiliou, and J. Rodriguez-Quintero, Phys.Rev. **D80**, 085018 (2009), 0906.2633.
 - [21] A. Courtoy, S. Scopetta, and V. Vento, Eur.Phys.J. **A47**, 49 (2011), 1102.1599.
 - [22] A. Courtoy, Int.J.Mod.Phys.Conf.Ser. **04**, 216 (2011), 1107.4880.
 - [23] Y. Liang et al. (Jefferson Lab Hall C E94-110 Collaboration) (2004), nucl-ex/0410027.
 - [24] P. Monaghan, A. Accardi, M. Christy, C. Keppel, W. Melnitchouk, et al. (2012), 1209.4542.
 - [25] L. Whitlow, E. Riordan, S. Dasu, S. Rock, and A. Bodek, Phys.Lett. **B282**, 475 (1992).
 - [26] A. De Rujula, H. Georgi, and H. D. Politzer, Annals Phys. **103**, 315 (1977).
 - [27] F. E. Close and Q. Zhao, Phys.Rev. **D66**, 054001 (2002), hep-ph/0202181.
 - [28] S. Jeschonnek and J. Van Orden, Phys.Rev. **D69**, 054006 (2004), hep-ph/0310298.
 - [29] L. Jenkovszky, V. Magas, J. Londergan, and A. Szczepaniak, Int.J.Mod.Phys. **A27**, 1250157 (2012), 1204.2216.
 - [30] S. Liuti, R. Ent, C. Keppel, and I. Niculescu, Phys.Rev.Lett. **89**, 162001 (2002), hep-ph/0111063.
 - [31] A. Martin, W. Stirling, R. Thorne, and G. Watt, Eur.Phys.J. **C63**, 189 (2009), 0901.0002.
 - [32] J. Pumplin, D. Stump, J. Huston, H. Lai, P. M. Nadolsky, et al., JHEP **0207**, 012 (2002), hep-ph/0201195.
 - [33] M. Gluck, P. Jimenez-Delgado, and E. Reya, Eur.Phys.J. **C53**, 355 (2008), 0709.0614.

- [34] H. Georgi and H. D. Politzer, Phys.Rev. **D14**, 1829 (1976).
- [35] I. Schienbein, V. A. Radescu, G. Zeller, M. E. Christy, C. Keppel, et al., J.Phys. **G35**, 053101 (2008), 0709.1775.
- [36] S. Alekhin, S. A. Kulagin, and S. Liuti, Phys.Rev. **D69**, 114009 (2004), hep-ph/0304210.
- [37] A. Accardi and J.-W. Qiu, JHEP **0807**, 090 (2008), 0805.1496.
- [38] R. Roberts, *The Structure of the proton: Deep inelastic scattering* (Cambridge monographs on mathematical physics, Cambridge, UK, 1990), univ. pr. ed.
- [39] D. Amati, A. Bassetto, M. Ciafaloni, G. Marchesini, and G. Veneziano, Nucl.Phys. **B173**, 429 (1980).
- [40] R. Roberts, Eur.Phys.J. **C10**, 697 (1999), hep-ph/9904317.
- [41] M. Pennington and G. G. Ross, Phys.Lett. **B102**, 167 (1981).
- [42] I. Niculescu, C. Keppel, S. Liuti, and G. Niculescu, Phys.Rev. **D60**, 094001 (1999).
- [43] I. Niculescu, C. Armstrong, J. Arrington, K. Assamagan, O. Baker, et al., Phys.Rev.Lett. **85**, 1186 (2000).
- [44] A. Deur, Private Communication (2013).
- [45] A. Deur, V. Burkert, J.-P. Chen, and W. Korsch, Phys.Lett. **B650**, 244 (2007), hep-ph/0509113.
- [46] A. Deur, V. Burkert, J. Chen, and W. Korsch, Phys.Lett. **B665**, 349 (2008), 0803.4119.
- [47] S. J. Brodsky, G. F. de Teramond, and A. Deur, Phys.Rev. **D81**, 096010 (2010), 1002.3948.
- [48] G. Grunberg, Phys.Lett. **B95**, 70 (1980).
- [49] G. Grunberg, Phys.Rev. **D29**, 2315 (1984).